

SCIENTIFIC REPORTS



OPEN

Targeted Patching and Dendritic Ca²⁺ Imaging in Nonhuman Primate Brain *in vivo*

Ran Ding^{1,2}, Xiang Liao^{1,2}, Jingcheng Li², Jianxiong Zhang², Meng Wang², Yu Guang², Han Qin², Xingyi Li², Kuan Zhang², Shanshan Liang², Jiangheng Guan², Jia Lou², Hongbo Jia³, Bingbo Chen⁴, Hui Shen¹ & Xiaowei Chen^{2,5}

Nonhuman primates provide an important model not only for understanding human brain but also for translational research in neurological and psychiatric disorders. However, many high-resolution techniques for recording neural activity *in vivo* that were initially established for rodents have not been yet applied to the nonhuman primate brain. Here, we introduce a combination of two-photon targeted patching and dendritic Ca²⁺ imaging to the neocortex of adult common marmoset, an invaluable primate model for neuroscience research. Using targeted patching, we show both spontaneous and sensory-evoked intracellular dynamics of visually identified neurons in the marmoset cortex. Using two-photon Ca²⁺ imaging and intracellular pharmacological manipulation, we report both action-potential-associated global and synaptically-evoked NMDA (N-methyl-D-aspartate) receptor-mediated local Ca²⁺ signals in dendrites and spines of the superficial-layer cortical neurons. Therefore, we demonstrate the presence of synaptic Ca²⁺ signals in neuronal dendrites in living nonhuman primates. This work represents a proof-of-principle for exploring the primate brain functions *in vivo* by monitoring neural activity and morphology at a subcellular resolution.

The use of nonhuman primates along with rodents in neuroscience research is pivotal for understanding human brain and diseases. Two-photon Ca²⁺ imaging together with patch-clamp recordings allows for elucidating the brain functions *in vivo* at multiple spatial scales ranging from neural populations to individual synapses^{1–3}. However, these sophisticated techniques for high-resolution mapping of brain structures and activities were initially developed for rodents and have not been fully available for primate brain research. Recently, *in vivo* two-photon imaging of neuronal activities at the population level with a single-cell resolution has been applied to the monkey neocortex^{4–7}, but imaging activities of single synapses, particularly those represent synaptic input-related signals^{1,3,8}, still remains a major challenge in nonhuman primates.

Neuronal dendrites compute both electrical and chemical signals, a process that is essential for information processing and communication in the brain. One of the most commonly used approaches for analyzing the dendritic signals is to image the dynamics of intracellular Ca²⁺ concentration^{3,9}. Rapid advances in two-photon microscopy and improved fluorescent Ca²⁺ indicators have enabled us to study the dendritic signals under both *in vitro*^{10,11} and *in vivo* conditions^{1,12–15}. Using such approaches, several studies have identified sensory-evoked local dendritic Ca²⁺ signals in different sensory cortex regions (visual, auditory, and barrel cortices) in mice and revealed a heterogeneous distribution of sensory inputs on neuronal dendrites^{1,3,14,16}. In contrast, recent two-photon imaging work has also identified the functional clustering of synaptic inputs in ferret visual cortex¹⁷. However, the knowledge of dendritic organization of sensory inputs in the primate brain neurons remains less clear. An essential step forward in addressing this question is to establish a proper technical approach to resolve

¹School of Biomedical Engineering, Tianjin Medical University, Tianjin, China. ²Brain Research Center, Third Military Medical University, Chongqing, China. ³Brain Research Instrument Innovation Center, Suzhou Institute of Biomedical Engineering and Technology, Chinese Academy of Sciences, Suzhou, China. ⁴Laboratory Animal Center, Third Military Medical University, Chongqing, China. ⁵CAS Center for Excellence in Brain Science and Intelligence Technology, Shanghai Institutes for Biological Sciences, Chinese Academy of Sciences, Shanghai, China. Ran Ding, Xiang Liao and Jingcheng Li contributed equally to this work. Correspondence and requests for materials should be addressed to B.C. (email: chenbb81@126.com) or H.S. (email: shenhui@tmu.edu.cn) or X.C. (email: xiaowei_chen@tmmu.edu.cn)

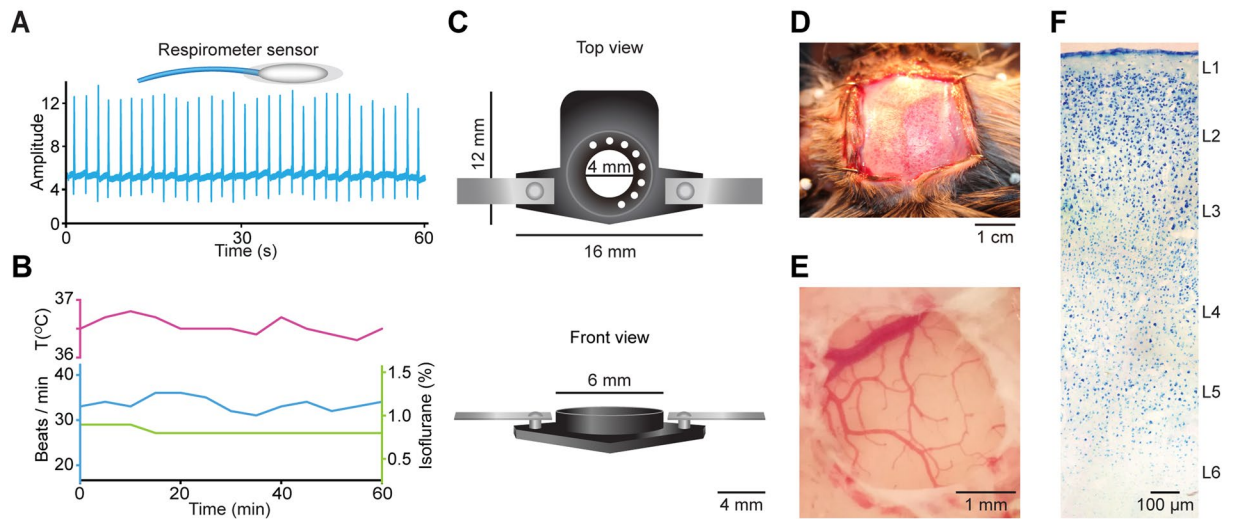


Figure 1. The Marmoset's physical condition and preparation for two-photon Ca^{2+} imaging in marmoset cortex *in vivo*. **(A)** Respiration rate recording. Upper, Cartoon of the sensor of respirometer. Lower, respiration activity over a 60 sec recording period. **(B)** Body temperature (upper, purple), breathing rate (middle, blue) and isoflurane concentration (lower, green) over a 60 min recording period. **(C)** Cartoon of the custom-made chamber (black part: length 16 mm, width 12 mm, innerdiameter 4 mm; outer diameter 6 mm; height 5 mm) and holder (grey part, length 10 mm for one side). Upper, top view. Lower, front view. **(D)** Exposed skull. **(E)** Exposed primary somatosensory cortex. **(F)** Nissl staining of the marmoset neocortex, showing all 6 layers (L).

subthreshold sensory-evoked input signals in the dendrites of primates *in vivo*. Alternatively, one can also apply the techniques that have been already developed in rodents to the primate brain.

In rodent brains, the successful implementation of *in vivo* imaging of neural activity in single dendritic spines, small membranous protrusions in dendrites that correspond to individual afferent excitatory synapses, has benefited from the use of high-speed two-photon imaging termed low power temporal oversampling (LOTOS) procedure^{1,18,19} or the use of a new generation of genetically encoded Ca^{2+} indicators (GCaMP6s)¹⁵. Alternatively, conventional two-photon imaging has also been used for *in vivo* spine Ca^{2+} imaging, but this was only achieved when the membrane potentials of the recorded neurons were strongly depolarized to -30 mV to 0 mV to maximize the NMDA receptor-dependent Ca^{2+} responses²⁰. In monkey cortex, *in vivo* imaging of dendritic spines has been restricted to the study of their morphology and turnover⁷. In the present study, to image the activities of dendrites and spines in primate brain, we chose to use the LOTOS procedure in conjunction with whole-cell patch-clamp recordings in the adult marmoset neocortex. Moreover, we chose to use a synthetic Ca^{2+} dye, as it offers a practical advantage over genetically encoded Ca^{2+} indicators, namely an easy-to-deliver property through the patch electrode². As a result, we were able to simultaneously monitor intracellular electrical signals from the soma and Ca^{2+} signals from the dendrites of visually identified neurons in the marmoset brain *in vivo*.

Materials and Methods

Animals. Two male common marmosets (*Callithrix jacchus*; 58 and 60 months old; body weight: 290 g and 300 g, respectively) were provided by the Laboratory Animal Center at the Third Military Medical University. The colony room is maintained at a temperature range of 27°C – 29°C and a relative humidity of 50–60%, with a 12L:12D light cycle. Marmosets live in family groups. They were fed with fruits and vegetables, accessed to water ad libitum. In the experiment day, peanuts and dried fruits were used to attract them to move to a transfer cage or an anesthesia cage. The marmosets were not used for other experiments before surgery and anesthesia. All experimental procedures were performed in accordance with institutional animal welfare guidelines and were approved by the Third Military Medical University Animal Care and Use Committee.

Surgery. Marmosets were anesthetized by 1.5% isoflurane with pure oxygen, and kept in a stereotaxic apparatus with a heating pad setting to 38 – 39°C in a prone position. We monitored the anesthesia state independently and the level of anesthesia was confirmed by the absence of tail-pinch or paw reflexes. The whole procedure of anesthesia was performed by a clinical certified anesthetist. The concentration of isoflurane was stable (Fig. 1) and was adjusted slightly and carefully only in accordance with the state of the animal. The surgical procedures were performed under aseptic environment. Ampicillin (40 mg kg^{-1}) and carprofen (5 mg kg^{-1}) were injected intramuscularly. Rectal temperature and breathing rate were monitored throughout the procedure (Fig. 1A,B). The fur and skin over parietal skull were removed after local lidocaine injection (2%). A custom-made plastic chamber was then fixed to the skull with cyanoacrylic glue (UHU) and dental cement (Tetric EvoFlow from Ivoclar Vivadent Corporate) over the left primary somatosensory cortex according to stereotaxic coordinates^{21,22} (Fig. 1C–E). We used a cranial drill to make a circular craniotomy (~ 3 mm diameter). The dura mater was removed by a forceps and the exposed cortex was covered with 1.5% low-melting-point agarose. Afterwards, the

marmoset was transferred and fixed on the recording setup. Unfortunately, one marmoset died around one hour after we transferred it to the recording setup, which was probably due to a high level of isoflurane (1.2–1.5%). Therefore, for another animal, we reduced the level to 0.6–0.8% throughout the entire experiments. In this condition, the breathing rate was stabilized in the range of 30–40 breaths per min (Fig. 1A,B). The recording chamber was perfused with normal artificial cerebral spinal fluid (ACSF) containing 125 mM NaCl, 4.5 mM KCl, 26 mM NaHCO₃, 1.25 mM NaH₂PO₄, 2 mM CaCl₂, 1 mM MgCl₂ and 20 mM glucose (pH 7.4 when bubbled with 95% oxygen and 5% CO₂). The rectal temperature of marmoset was kept between 36.5–37.5 °C throughout the experiments (Fig. 1B).

Two-Photon Ca²⁺ Imaging. Two-photon imaging was performed with a custom-built two-photon microscope system based on 12 kHz resonant scanner (model “LotosScan 1.0”, Suzhou Institute of Biomedical Engineering and Technology), similar to that described previously^{14,16} (Jia *et al.*¹⁴; Varga *et al.*¹⁶). Two-photon excitation light was delivered by a mode-locked Ti:Sa laser (model “Mai-Tai DeepSee”, Spectra Physics), and a 40 × /0.8 NA water-immersion objective (Nikon) was used for imaging. For Ca²⁺ imaging experiments, the excitation wavelength was set to 920 nm. For somatic and dendritic Ca²⁺ imaging, we acquired images of 600 × 600 pixels at 40 Hz frame rate. The size of field-of-view was ~ 200 μm × 200 μm. The average power delivered to the brain ranged from 30 to 80 mW, depending on the depth of imaging. For spine Ca²⁺ imaging, we changed the imaging system to the LOTOS scanning mode^{1,15,16,18}. We reduced the number of lines to 64 and the number of pixels in each line to 256. The imaging repetition rate was 200 Hz. The width of the field-of-view was therefore reduced to 27–42 μm. The average power delivered to the brain was 15–30 mW. Within an imaging time window of ~5 min for each dendritic field, no sign of photodamage was observed.

Hind-limb Electrical Stimulation. For hind-limb electrical stimulation, electrical stimulation (duration 1 s, intensity 0.1–0.6 mA) was delivered to the hind-paws through two 30-gauge needles connected to an isolated pulse stimulator (Isolated Pulse Stimulator Model 2100, AM-system).

Whole-Cell Patch-Clamp Recordings. For whole-cell patch-clamp recordings in marmoset primary somatosensory cortex neurons *in vivo*, we used the “shadowpatching” procedure according to the previous studies^{1,23}. Recordings were done with an EPC10 amplifier (USB double, HEKA Elektronik). Electrophysiological data were filtered at 10 kHz and sampled at 20 kHz using Patchmaster software (HEKA). The pipette electrodes pulled from borosilicate glass capillaries (BF150–86–10, Sutter Instrument Company, Novato, CA) had a resistance of 4–6 MΩ when filled with internal solution containing 112 mM potassium gluconate, 8 mM KCl, 10 mM HEPES, 4 mM Mg-ATP, 0.375 mM Na₂GTP, 10 mM sodium phosphocreatine and OGB-1 potassium salt (200 μM; Invitrogen). The patch pipette penetrated the pia mater with positive pressure of 100–200 mbar and was then reduced to ~ 20–30 mbar to obtain good images of both electrode and shadow neurons under two-photon imaging (Fig. 2A–C). After identification of the cell of interest, the tip of the pipette electrode pushed against its membrane. When the tip resistance raised 3–5 MΩ, we released positive pressure and suctioned to obtain a gigaohm seal. After gigaohm seal formation, gentle suction was applied to break through the cell membrane to establish whole-cell configuration (Fig. 2D). The recording of the best two cells lasted up to ~2 hours and the recording duration of other eight cells varied from 30 minutes to 1 hour). For intracellular pharmacological manipulation, we included MK-801 (1 mM) in the internal solution. The series resistance was continuously monitored and the data were rejected for analysis if the resistance was higher than 30 MΩ. Dendritic Ca²⁺ imaging was started at least 20 min after formation of whole-cell configuration. The experiments were done in one session lasting 17 hours. The state of the animal was stable (body temperature: 36.5 °C; respiration rate: 30–40 breaths per min) and carefully monitored until the end of the recording session.

Nissl Staining. After imaging and electrophysiological experiments, the marmoset was deeply anesthetized by an intraperitoneal injection of sodium pentobarbital and perfused transcardially with 0.9% NaCl, followed by fixation with 4% paraformaldehyde in 0.1 M PBS (pH 7.4). The animal was carefully euthanized in accordance with institutional animal welfare guidelines, and it was approved by the Third Military Medical University Animal Care and Use Committee. The cryoprotected marmoset brain was sliced with a thickness of 40–50 μm. The slices were rehydrated and stained in 0.1% cresyl violet solution for 3–10 minutes. Then, they were soaked in 95% ethyl alcohol for 5–30 minutes, dehydrated in 100% alcohol and cleared in xylene for 5 minutes. At last, the imaging was obtained with a stereoscope (Olympus) (Fig. 1F).

Data Analysis. The analyses of electrophysiological and Ca²⁺ imaging data were conducted offline by using custom-written software in LabVIEW 2012 (National Instruments), Igor Pro 5.0 (Wavemetrics) and Matlab 8 (Mathworks). For correcting lateral motion in the imaging data, a rigid-body transformation based frame-by-frame alignment was applied by using Turboreg software (ImageJ plugin). For reconstructing morphology of the recorded neuron, the fluorescent image projections of the single neuron were generated from z-stack of two-photon images using Simple Neurite Tracer software (ImageJ, <http://rsb.info.nih.gov/ij/>), and then the dendrites were manually tracked using Adobe Illustrator CS6 (Adobe Systems).

To extract fluorescence signals from imaging data, regions of interests (ROIs) were visually identified and drawn based on fluorescence intensity. All pixels within each specified ROI were averaged to estimate fluorescence changes (f). Relative fluorescence changes $\Delta f/f = (f - f_0)/f_0$ were calculated as Ca²⁺ signals, where the baseline fluorescence of the ROI f_0 was estimated as the 25th percentile of the fluorescence within a sliding time window (window size: 10 s). Regions of interest for spine calcium imaging analyses were restricted to the clearly visible protrusions emanating laterally from the dendritic shaft, as described previously^{1,18,19}. To remove the noises from respiration (rate = 0.5–0.6 Hz) and heartbeat (rate = 4–5 Hz)²⁴, the $\Delta f/f$ traces shown in all figures were first notch filtered (0.6 and 4 Hz) and then low-pass filtered (0–5 Hz) with Butterworth filter (3rd order).

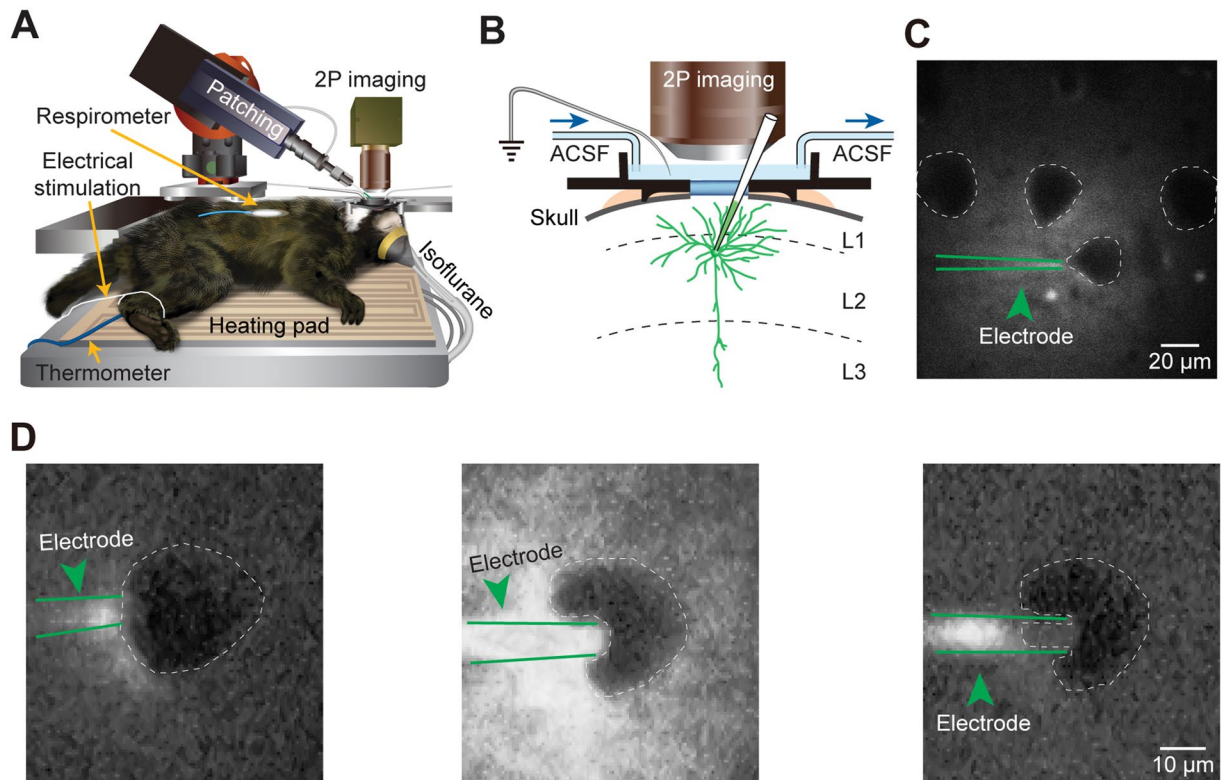


Figure 2. Two-photon targeted whole-cell recordings in marmoset cortical neurons *in vivo*. **(A)** Schematic of two-photon imaging and whole-cell recording in a marmoset anesthetized with isoflurane. The yellow arrows point to the respirometer sensor, the thermometer and the wire of electrical stimulation. **(B)** Side view of the experimental arrangement, showing the patch electrode filled with OGB-1, the water-immersion objective, the agarose-covered cortical surface, the recording chamber, and the flow direction of ACSF perfusion into the cortical surface. **(C)** OGB-1 was blown out from an electrode and the neurons can be identified as shadows which were delineated with white dotted contours. The electrode is pointed by a green arrowhead and delineated with green lines. **(D)** The process of obtaining whole-cell configuration. Left, the electrode was approaching the shadow. Middle, the neuron was pressed by the pipette positive pressure. Right, the pressure was released and suction was applied to the pipette to form a gigohm seal.

Summarized data were presented in figures as mean \pm standard error of the mean (SEM). To compare data from two groups, we used Wilcoxon rank sum test to determine statistical significance between them. $P < 0.05$ was considered statistically significant.

Results

Intracellular Dynamics of Marmoset Cortical Neurons Revealed by Two-Photon Guided Whole-Cell Recordings.

We performed targeted whole-cell recordings using the “shadowpatching” procedure^{1,23} in the hind-limb region of the marmoset somatosensory cortex under isoflurane anesthesia (Fig. 2A). By means of two-photon imaging through a cranial window, we patched neurons under direct visual control with a glass electrode containing the Ca^{2+} -sensitive fluorescent dye Oregon Green BAPTA-1 (OGB-1). The somata of the patched neurons were located in the superficial layer at a depth of 120–300 μm , corresponding to the neurons within layer 2 (Figs 1F and 2B)^{25,26}. The most evident limitation of using this technique in deep layer neurons is the fact that the pipette would be contaminated more frequently since it needs to penetrate thicker tissues. This would significantly reduce the success rate of obtaining a high-quality patch-clamp recording. The neurons were passively loaded with the Ca^{2+} dye after achieving whole-cell configuration. At the end of recordings of each neuron, the morphology was reconstructed from z-stack of two-photon images, revealing a pattern of numerous apical, oblique and basal dendrites (see an example in Fig. 3A). Current-clamp recordings at the neuronal somata revealed slow oscillations of membrane potentials consisting of an alternation of depolarized (UP) and hyperpolarized (DOWN) states (UP state frequency was in the range of 0.52 to 0.76 Hz; 0.65 ± 0.07 Hz, $n = 7$ neurons; Fig. 3B, left panel), showing a bimodal distribution of membrane potentials (Fig. 3B, right panel). The membrane potentials at DOWN states ranged from -80 to -65 mV (-71 ± 2.2 mV, $n = 7$). The membrane potentials were not corrected for liquid junction potentials. Action potential (AP) firing was sparsely found during UP states (0.019 ± 0.004 Hz, $n = 7$, calculated from both UP and DOWN states). These properties are similar to those described for mouse superficial-layer cortical neurons under the same condition^{1,19}. Previous studies using extracellular recordings have suggested similar slow oscillations during slow-wave sleep²⁷. In addition, electrical stimulation of the hindlimb produced responses in the recorded neurons. Increasing stimulus intensity resulted

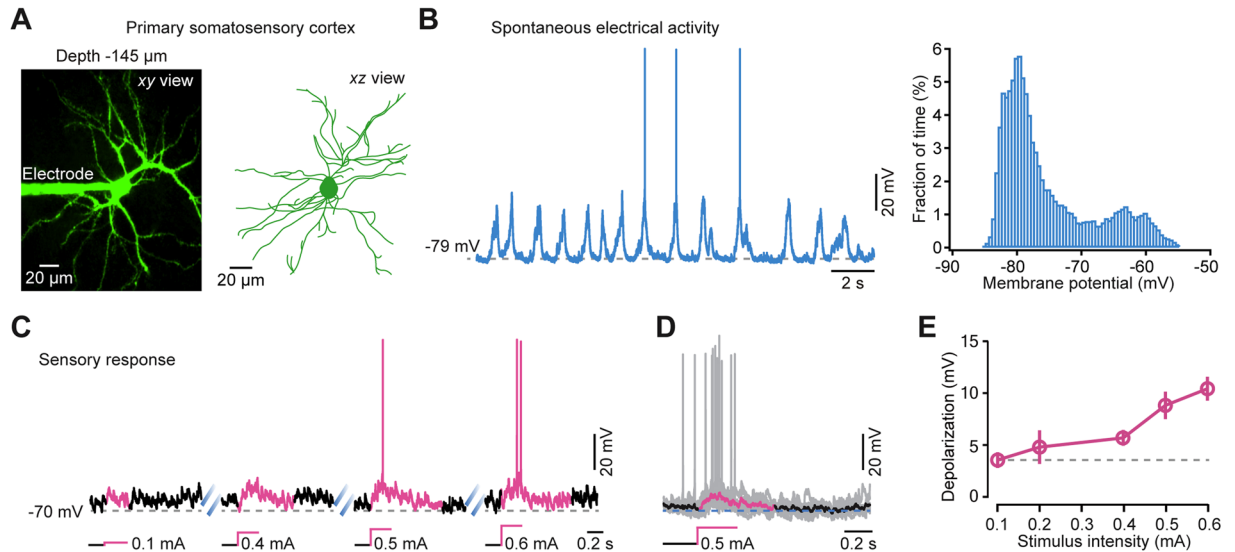


Figure 3. The spontaneous and stimulation-evoked electrical responses in marmoset cortical neurons. **(A)** Z-projection of *in vivo* two-photon images of a whole-cell patched layer 2 (L2) pyramidal cortical neuron. Left, top view of this neuron. Right, side view of the neuron reconstructed from two-photon images. **(B)** Left, representative whole-cell recording of spontaneous activity from the same L2 neuron as in panel **(A)** under anesthesia. Right, distribution of membrane potentials of this neuron during a 45 s recording period. **(C)** Neuronal responses to different intensities of electrical stimulation of the hind-limb from another neuron. **(D)** Overlay of sensory responses to 0.5 mA electrical stimulation from 7 traces. **(E)** Intensity dependence of stimulus-evoked depolarization ($n = 4$).

in a progressive increase in the amplitude of postsynaptic potential responses and reliably produced spiking when the stimulus was above 0.5 mA (Fig. 3C–E). Thus, we successfully establish targeted whole-cell recordings in the marmoset cortex, allowing for the analysis of intracellular dynamics of single identified neurons in the intact brains of nonhuman primates.

Action Potential-Associated Ca^{2+} Signals in the Dendrites of Marmoset Cortical Neurons. In combination of whole-cell recordings, we next performed two-photon imaging to explore back-propagating AP-associated dendritic Ca^{2+} signals in marmoset cortical neurons. We carried out imaging at a speed of 40 frames per second to achieve a resolution at the level of dendrites^{14,16}. Figure 4A,B show an example of such recordings, in which we obtained four different planes of focus from apical to basal dendrites in the same neuron. We observed that APs produced Ca^{2+} transients invading effectively all imaged dendritic branches. Even for single APs, we were able to detect these global dendritic Ca^{2+} signals. These global dendritic signals could be evoked by current injections through the patch electrode (Fig. 4B), indicating that such signals are largely resultant from the activation of voltage-gated Ca^{2+} channels by AP backpropagation, with a possible contribution of coincidentally-occurring local synaptic activation, consistent with the results from L2/3 neurons in mouse cortex *in vivo*^{1,19,28}. As indicated by quantitative analysis, the amplitude of AP-associated Ca^{2+} transients evoked by current injections showed a significant dependence on the number of APs (Fig. 4C; $n = 6$).

Subthreshold Ca^{2+} Signals in the Dendrites of Marmoset Cortical Neurons. In addition to the observation of AP-associated Ca^{2+} transients, in many occasions we also found local dendritic Ca^{2+} signals, probably representing the synaptic input signals through the activation of NMDA receptors^{14,16}. For example, in the plane of focus shown in Fig. 5A, several subthreshold Ca^{2+} transients spontaneously occurred in “dendrite 1” (ROI1), but not in “dendrite 2” (ROI2). In contrast, a single AP produced Ca^{2+} transients in both dendrites. Overall, such local dendritic Ca^{2+} transients were observed in 10 out of 22 dendrites ($n = 5$ neurons), which was less frequent than the results observed in mouse cortical neurons^{1,19}. Across all the imaged dendritic branches that had local Ca^{2+} signals, we found that their frequency was about 5 transients/min ($n = 10$ dendrites). Based on a number of studies performed in mouse cortical neurons both *in vitro*^{28,29} and *in vivo*^{1,14,16,30}, the major source of these local dendritic signals is synaptically-driven NMDAR-dependent Ca^{2+} entry. To confirm whether this is also true for marmoset cortical neurons, we intracellularly applied MK-801, a NMDA channel blocker, into the recorded neurons through the patch electrode. We observed that MK-801 completely abolished the local dendritic Ca^{2+} signals. However, the global dendritic Ca^{2+} signals evoked by current injection-induced AP backpropagation were still present, with a reduction in their amplitudes (Fig. 5B,C: right panels). It should be mentioned that MK-801 might affect the local circuit excitability as we moved the electrode through the tissue towards the cell.

Ca^{2+} Signals in Dendritic Spines of Marmoset Cortical Neurons. For imaging dendritic Ca^{2+} signals at the level of single spines, we switched the imaging system to the LOTOS scanning mode that has a repetition

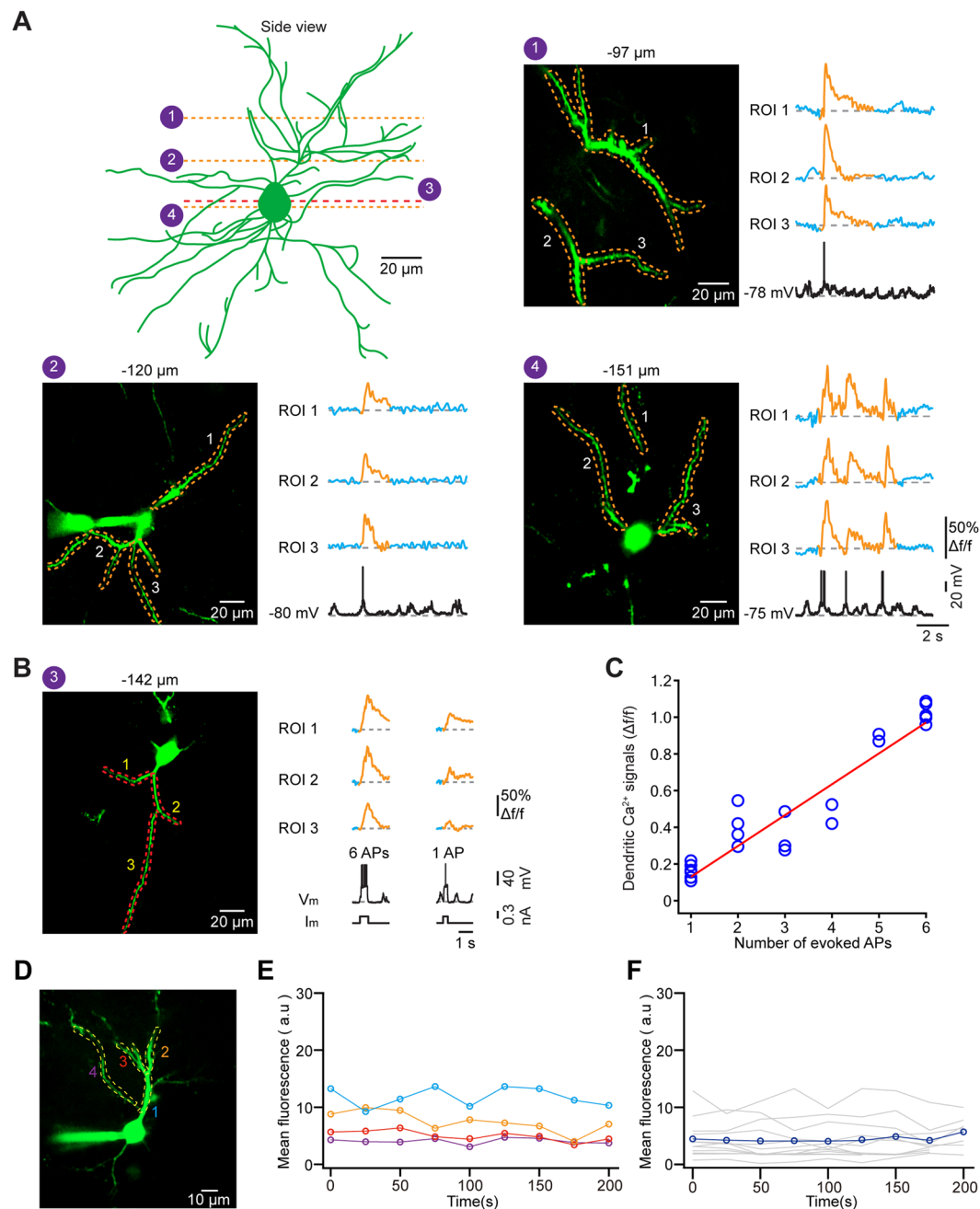


Figure 4. Global dendritic Ca^{2+} signals associated with action potentials. **(A)** Upper left panel, side view of a recorded neuron, the same as in Fig. 3A. Four different planes of focus are indicated by dotted lines. Three other panels, dendritic Ca^{2+} transients associated back-propagating action potentials (APs) in these three planes of this neuron. Each panel: left, two-photon image with regions of interest (ROIs); right, Ca^{2+} transients ($\Delta f/f$) from the corresponding ROIs and the somatic electrical activity. **(B)** Ca^{2+} transients from three ROIs during 6 APs and 1 AP that were evoked by current injections. Left, two-photon Ca^{2+} image with ROIs. Right, Ca^{2+} transients from these ROIs, and their corresponding membrane potentials (V_m) and current injections (I_m). **(C)** Dependence of amplitude of dendritic Ca^{2+} transients on the number of APs that were evoked by current injections. Each blue circle represents the result from one dendritic region of interest and the red line indicates a linear fit ($R^2 = 0.861$, $P = 0.0048$; $n = 6$ neurons). **(D)** Two-photon Ca^{2+} image with four ROIs from another cell. **(E)** Mean fluorescence from these ROIs during a 200 s recording. **(F)** Mean fluorescence from 13 different dendritic regions of three neurons.

speed of 200 frames/s and needs only a low excitation laser power per frame. Figure 5D shows an example of spine imaging, in which we observed Ca^{2+} transients only in “spine 1” (S1) in the absence of APs, without any detectable signals in the parent dendritic shaft (D1). However, other spines in this dendritic branch, for example

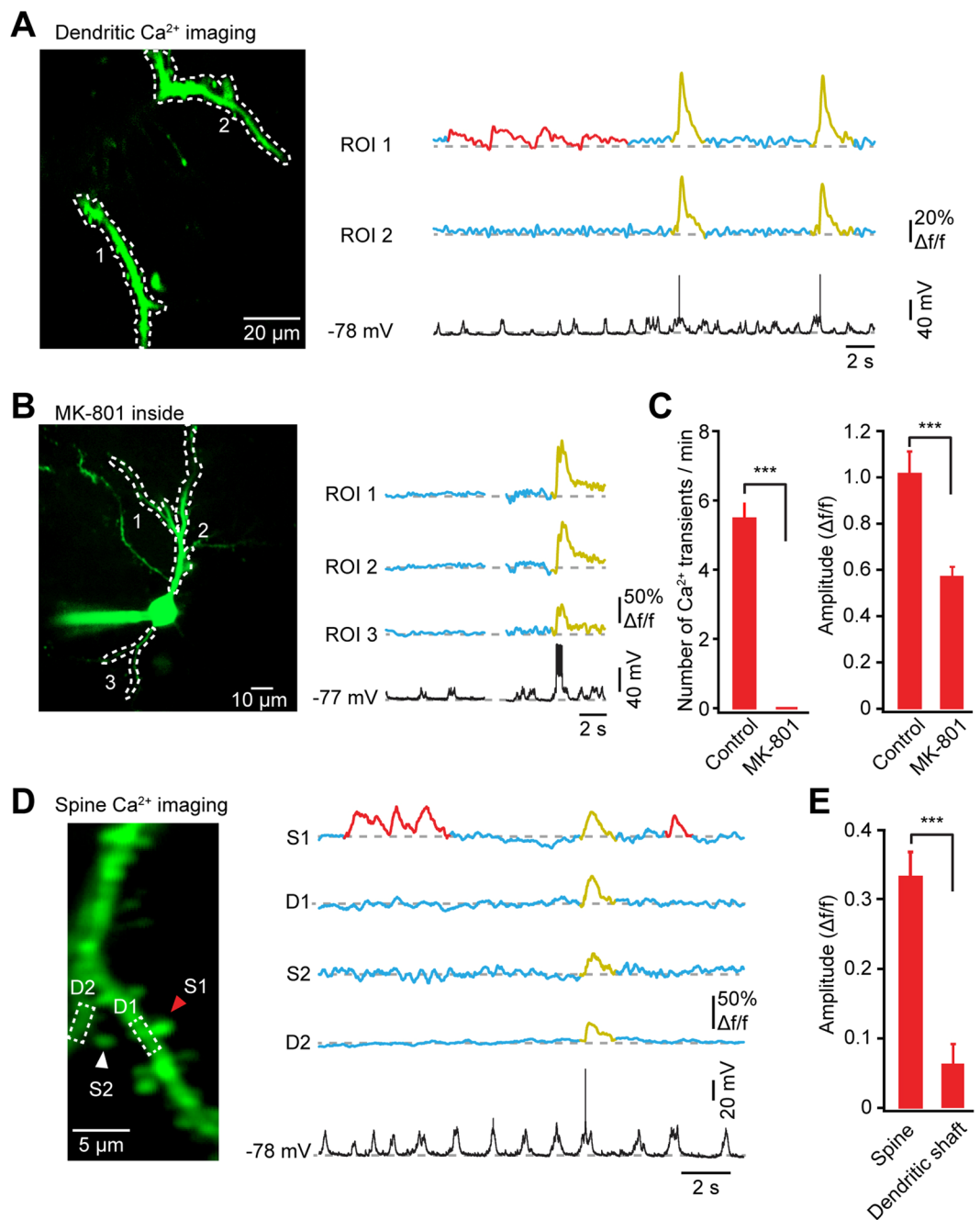


Figure 5. Local Ca²⁺ signals associated with synaptic activation in dendrites and spines. **(A)** Subthreshold local dendritic Ca²⁺ signals. Left, two-photon image with ROIs from the same neuron as in Fig. 3A. Right, local dendritic Ca²⁺ signals (in red) and AP-associated dendritic Ca²⁺ signals (in yellow), and their corresponding electrical signals recorded from the soma (in black). **(B)** Blockade of local dendritic Ca²⁺ signals by intracellularly applied MK-801 (1 mM). Note that AP-associated Ca²⁺ signals were still present, obtained from the same neuron in Fig. 4D. **(C)** Comparison of number of subthreshold dendritic Ca²⁺ transients (Left) and amplitude of single AP-associated dendritic Ca²⁺ transients (right) without (control: $n = 10$ dendrites from 5 neurons) and with MK-801 ($n = 8$ dendrites from 3 neurons). Wilcoxon rank sum test, *** $P < 0.001$. Error bar shows SEM. **(D)** Subthreshold spine Ca²⁺ signals. Left, two-photon image of a dendritic segment, obtained from the same neuron as in Fig. 3A. Right, Ca²⁺ signals from two spines (marked by arrowheads) and their dendritic shafts (outlined by dotted boxes) in this dendritic segment, and the corresponding somatic electrical signals. Local Ca²⁺ signals are marked in red, while AP-associated signals are marked in yellow. **(E)** Summary of the amplitude of local Ca²⁺ transients in spines and in their dendritic shafts (10 spines from 3 neurons). Wilcoxon signed rank test, *** $P < 0.001$.

“spine 2” (S2), did not show any subthreshold Ca^{2+} signals during the same period. As a control, an AP reliably produced Ca^{2+} transients in all ROIs. Overall, we found local Ca^{2+} signals in 10 spines, with no or smaller signals in their parent dendrites (Fig. 5E). These results demonstrate the recordings of synaptic Ca^{2+} signals in dendritic spines in marmoset cortical neurons.

Discussion

In this study, we have successfully adapted the technique used for investigating dendritic functions *in vivo* that was initially developed in mice^{1,18} to study a New World primate, common marmoset. In its cerebral cortex, we have provided a proof-of-principle for the establishment of two major challenging *in vivo* methods, including (1) targeted whole-cell patch-clamp recordings in visually identified neurons, and (2) two-photon Ca^{2+} imaging in neuronal dendrites.

Up to now, it still remains a great technical challenge to perform whole-cell patch-clamp recordings in monkey brain neurons *in vivo*. Whole-cell or intracellular membrane potential measurements have been just reported very recently in the cortex of awake monkeys through the use of blind patching procedure³¹ or the use of sharp electrodes³². As previously developed in the mouse cortex and cerebellum²³, the targeted patching allows for the effective control and recording of the membrane potentials or a rapid delivery of fluorescent indicator/plasmid DNA/pharmacological agent into visually identified neurons in the intact primate brain. Using this procedure, one can also easily obtain the morphological information of the recorded cells according to *in vivo* two-photon imaging-based 3D reconstruction. In the present study, we show the use of targeted patching in marmoset monkey cortex for the recording and control of the intracellular dynamics of neurons *in vivo*. Under isoflurane anesthesia, we find the presence of slow oscillations of membrane potentials, namely UP and DOWN states in marmoset cortical neurons. This type of membrane potential activity was often found to be prevalent in cortical neurons during slow-wave sleep or under anesthesia according to the results from different species, e.g. rodents and cats^{1,19,33}. However, owing to technical difficulty, in previous studies using extracellular recordings, these bistable membrane potentials of cortical neurons have been only inferred but not directly demonstrated to be existed in the marmosets^{27,34}. In addition, using whole-cell recordings, we have observed a stimulus intensity dependence of sensory-evoked intracellular responses in marmoset cortical neurons, which may provide a feasible tool for the study of cortical processing of sensory information at this level of resolution in nonhuman primate brain *in vivo*.

Using a combination of two-photon Ca^{2+} imaging and patch-clamp recordings, we have detected subthreshold synaptic Ca^{2+} transients in dendrites and spines in the marmoset cortical neurons. Intracellular pharmacological experiments reveal that these local synaptic Ca^{2+} transients are NMDA receptor-dependent. However, a recent study using an adeno-associated virus-based expression of GCaMP6 in the marmosets only reported global Ca^{2+} transients occurring throughout single dendritic branches³⁵, which probably reflected backpropagation of APs and/or dendritic spiking, although no electrophysiological recordings were simultaneously performed. The failure of detection of synaptic input signals in their study could be due to the much larger movement artifacts caused by heartbeats or respiration activity than those in the mouse cortex¹⁸. In our study, we overcame this issue by adding a thick layer of agarose. In addition, our single cell labeling through the patch pipette yielded lower background fluorescence than that with virus-based labeling of genetically encoded calcium indicators³⁵, which could significantly reduce the background contamination and thus improve the visibility of subthreshold dendritic signals. Therefore, our work extends the earlier study and can facilitate future investigations of mapping synaptic input signals in the neuronal dendrites in primate brain.

Since our imaging and electrophysiological recordings were done in one marmoset, this may raise concerns about the reliability, replicability and limitations of our approach. First, we obtained a total number of 10 whole-cell patched neurons from this animal. On average, no more than three attempts of inserting patch electrodes were needed to establish the whole-cell recording configuration. The recording time for each neuron was in the range of 30 minutes to 2 hours (two cells lasted up to ~2 hours and other eight cells varied from 30 minutes to 1 hour). The success rate of targeted whole-cell recording is not different from that was done in mice^{1,18}. However, experiments with this large animal involve some specific adaptations to achieve a successful recording. In particular, as compared to mice, we observed a slower and stronger respiration activity in marmosets (30–40 breaths per min in marmosets versus 90–120 breaths per min in mice)¹⁸, which produced much larger brain pulsations and thus became a major reason for the increased difficulty of targeted patching. This issue can be minimized by the use of an extra-thick layer of agarose (~3 mm), a large cranial window (~3 mm diameter), and, importantly, a very stable respiration control throughout the recordings by adjusting isoflurane at a relatively low level (0.6–0.8%). Second, dye filling using a patch electrode often suffers from dye leakage and insufficient filling of distant dendrites. Indeed, overall, only six out of ten recorded neurons had distant dendrites (defined as those at ~200 μm from their soma) clearly labelled with the Ca^{2+} dye. To minimize this problem, we restricted our dendritic analyses to the clearly visible dendrites of these neurons. In addition, to assure a sufficient dye filling, we restricted our series resistance of patch electrode to <30 M Ω and started dendritic imaging at least 20 min after formation of whole-cell configuration. Third, our approach provides the unique means to study single-cell behavior in detail without gaining much insight into the functions of the network it is connected to. Multicell bolus loading of synthetic calcium dyes³⁶ or the use of virus-based labeling of genetically encoded calcium sensors¹⁵, together with single-cell patch-clamp recordings, may help to study single cells in the context of their network. Fourth, as compared to the use of GCaMP6s or other genetically encoded calcium indicators, our approach does not allow for recording the same neurons for days and weeks. Finally, this is a proof-of-principle report for the method that was performed in an anesthetized marmoset, which contains only limited amount of data. Based on these preliminary results, we did not observe any clear marmoset-specific properties. The future identification

of any species-specific signature in the marmoset cortex requires more systematic investigations with delivering stimulation of different sensory features or under the conditions of higher order or complex behaviors.

We used the marmoset, as it has been recently received world-wide attention and is an excellent primate model for brain research due to its small brain size, high reproductive efficiency and availability of transgenic technologies^{37,38}. In particular, the smooth brain surface of marmosets affords huge advantages over other primate models for optical imaging and electrode penetration^{7,35,39}. In addition, marmosets share many similarities in cognitive functions and social behavioral features with humans due to common descent^{39,40}. Therefore, functional recordings of the marmoset brain neurons using high-resolution technologies should shed light on the understanding of the human brain and also for the development of strategies for the diagnosis and therapy of psychiatric and neurological disorders^{38,41}. The procedure we demonstrated here would be a valuable addition to the toolbox for high-resolution functional recordings, particularly for acute experiments.

In conclusion, a combination of targeted patching and two-photon Ca^{2+} imaging of dendrites/dendritic spines will provide a useful tool to study single-neuron physiology, particularly how single neurons integrate sensory inputs through their dendrites^{1,3,14}, in the entire primate brain networks under both healthy and diseased conditions. Although our recordings were done under anesthesia, this method can be possibly adapted to the awake primates in future.

References

- Chen, X., Leischner, U., Rochefort, N. L., Nelken, I. & Konnerth, A. Functional mapping of single spines in cortical neurons *in vivo*. *Nature* **475**, 501–505 (2011).
- Grienberger, C. & Konnerth, A. Imaging calcium in neurons. *Neuron* **73**, 862–885 (2012).
- Grienberger, C., Chen, X. & Konnerth, A. Dendritic function *in vivo*. *Trends in Neurosciences* **38**, 45–54 (2015).
- Heider, B., Nathanson, J. L., Isacoff, E. Y., Callaway, E. M. & Siegel, R. M. Two-photon imaging of calcium in virally transfected striate cortical neurons of behaving monkey. *PLoS One* **5**, e13829 (2010).
- Nauhaus, I., Nielsen, K. J., Disney, A. A. & Callaway, E. M. Orthogonal micro-organization of orientation and spatial frequency in primate primary visual cortex. *Nat Neurosci* **15**, 1683–1690 (2012).
- Ikezo, K., Mori, Y., Kitamura, K., Tamura, H. & Fujita, I. Relationship between the local structure of orientation map and the strength of orientation tuning of neurons in monkey V1: a 2-photon calcium imaging study. *J Neurosci* **33**, 16818–16827 (2013).
- Sadakane, O. *et al.* *In Vivo* Two-Photon Imaging of Dendritic Spines in Marmoset Neocortex. *eNeuro* **2**, doi:10.1523/eneuro.0019-15.2015 (2015).
- London, M. & Häusser, M. Dendritic computation. *Annu Rev Neurosci* **28**, 503–532 (2005).
- Bloodgood, B. L. & Sabatini, B. L. Ca^{2+} signaling in dendritic spines. *Curr Opin Neurobiol* **17**, 345–351 (2007).
- Yuste, R. & Denk, W. Dendritic spines as basic functional units of neuronal integration. *Nature* **375**, 682–684 (1995).
- Nevian, T. & Sakmann, B. Spine Ca^{2+} signaling in spike-timing-dependent plasticity. *J Neurosci* **26**, 11001–11013 (2006).
- Svoboda, K., Denk, W., Kleinfeld, D. & Tank, D. W. *In vivo* dendritic calcium dynamics in neocortical pyramidal neurons. *Nature* **385**, 161–165 (1997).
- Helmchen, F., Svoboda, K., Denk, W. & Tank, D. W. *In vivo* dendritic calcium dynamics in deep-layer cortical pyramidal neurons. *Nat Neurosci* **2**, 989–996 (1999).
- Jia, H., Rochefort, N. L., Chen, X. & Konnerth, A. Dendritic organization of sensory input to cortical neurons *in vivo*. *Nature* **464**, 1307–1312 (2010).
- Chen, T. W. *et al.* Ultrasensitive fluorescent proteins for imaging neuronal activity. *Nature* **499**, 295–300 (2013).
- Varga, Z., Jia, H., Sakmann, B. & Konnerth, A. Dendritic coding of multiple sensory inputs in single cortical neurons *in vivo*. *Proc Natl Acad Sci USA* **108**, 15420–15425 (2011).
- Wilson, D. E., Whitney, D. E., Scholl, B. & Fitzpatrick, D. Orientation selectivity and the functional clustering of synaptic inputs in primary visual cortex. *Nat Neurosci* **19**, 1003–1009 (2016).
- Chen, X. *et al.* LOTOS-based two-photon calcium imaging of dendritic spines *in vivo*. *Nat Protoc* **7**, 1818–1829 (2012).
- Chen, X., Rochefort, N. L., Sakmann, B. & Konnerth, A. Reactivation of the same synapses during spontaneous up states and sensory stimuli. *Cell Rep* **4**, 31–39 (2013).
- Takahashi, N. *et al.* Locally synchronized synaptic inputs. *Science* **335**, 353–356 (2012).
- Krubitzer, L. A. & Kaas, J. H. The organization and connections of somatosensory cortex in marmosets. *J Neurosci* **10**, 952–974 (1990).
- Paxinos, G., Watson, C., Petrides, M., Rosa, M. & Tokuno, H. *The Marmoset Brain in Stereotaxic Coordinates* (Academic Press/Elsevier, 2012).
- Kitamura, K., Judkewitz, B., Kano, M., Denk, W. & Häusser, M. Targeted patch-clamp recordings and single-cell electroporation of unlabeled neurons *in vivo*. *Nat Methods* **5**, 61–67 (2008).
- Mundinano, I. C., Flecknell, P. A. & Bourne, J. A. MRI-guided stereotaxic brain surgery in the infant and adult common marmoset. *Nat Protoc* **11**, 1299–1308 (2016).
- Elston, G. N., Rosa, M. G. & Calford, M. B. Comparison of dendritic fields of layer III pyramidal neurons in striate and extrastriate visual areas of the marmoset: a Lucifer yellow intracellular injection. *Cereb Cortex* **6**, 807–813 (1996).
- Watakabe, A. *et al.* Comparative analyses of adeno-associated viral vector serotypes 1, 2, 5, 8 and 9 in marmoset, mouse and macaque cerebral cortex. *Neurosci Res* **93**, 144–157 (2015).
- Issa, E. B. & Wang, X. Sensory responses during sleep in primate primary and secondary auditory cortex. *J Neurosci* **28**, 14467–14480 (2008).
- Koester, H. J. & Sakmann, B. Calcium dynamics associated with action potentials in single nerve terminals of pyramidal cells in layer 2/3 of the young rat neocortex. *J Physiol* **529**, 3, 625–646 (2000).
- Higley, M. J. & Sabatini, B. L. Calcium signaling in dendritic spines. *Cold Spring Harb Perspect Biol* **4**, a005686 (2012).
- Waters, J., Larkum, M., Sakmann, B. & Helmchen, F. Supralinear Ca^{2+} influx into dendritic tufts of layer 2/3 neocortical pyramidal neurons *in vitro* and *in vivo*. *J Neurosci* **23**, 8558–8567 (2003).
- Tan, A. Y., Chen, Y., Scholl, B., Seidemann, E. & Priebe, N. J. Sensory stimulation shifts visual cortex from synchronous to asynchronous states. *Nature* **509**, 226–229 (2014).
- Gao, L., Kostlan, K., Wang, Y. & Wang, X. Distinct Subthreshold Mechanisms Underlying Rate-Coding Principles in Primate Auditory Cortex. *Neuron* **91**, 905–919 (2016).
- Steriade, M., Nunez, A. & Amzica, F. A novel slow (<1 Hz) oscillation of neocortical neurons *in vivo*: depolarizing and hyperpolarizing components. *J Neurosci* **13**, 3252–3265 (1993).
- Issa, E. B. & Wang, X. Altered neural responses to sounds in primate primary auditory cortex during slow-wave sleep. *J Neurosci* **31**, 2965–2973 (2011).

35. Sadakane, O. *et al.* Long-Term Two-Photon Calcium Imaging of Neuronal Populations with Subcellular Resolution in Adult Non-human Primates. *Cell Rep* **13**, 1989–1999 (2015).
36. Stosiek, C., Garaschuk, O., Holthoff, K. & Konnerth, A. *In vivo* two-photon calcium imaging of neuronal networks. *Proc Natl Acad Sci USA* **100**, 7319–7324 (2003).
37. Sasaki, E. *et al.* Generation of transgenic non-human primates with germline transmission. *Nature* **459**, 523–527 (2009).
38. Okano, H. & Mitra, P. Brain-mapping projects using the common marmoset. *Neurosci Res* **93**, 3–7 (2015).
39. Mitchell, J. F. & Leopold, D. A. The marmoset monkey as a model for visual neuroscience. *Neurosci Res* **93**, 20–46 (2015).
40. Burkart, J. M. & Finkenwirth, C. Marmosets as model species in neuroscience and evolutionary anthropology. *Neurosci Res* **93**, 8–19 (2015).
41. Cyranoski, D. Marmosets are stars of Japan's ambitious brain project. *Nature* **514**, 151–152 (2014).

Acknowledgements

We thank Y. Sun. and L. Xiao for technical assistance in Nissl staining. This work was supported by grants from the 1000 Talents Program for Young Scholars, the Nature Science Foundation of China (No. 31572350, 31400933, 81671106) and the National Basic Research Program of China (“973 Program”: 2015CB759500, 2014CB541600). X.C. is a junior fellow of the CAS Center for Excellence in Brain Science and Intelligence Technology.

Author Contributions

R.D., X.L., J.L., B.C., H.S. and X.C. designed the experiments. R.D., X.L., J.L., M.W., Y.G., J.Z., H.Q., X.C. performed the two-photon imaging and electrophysiological experiments. J.Z. and K.Z. performed the Nissl staining. X.L. and B.C. established the protocol for anesthesia and surgery. R.D., X.L., J.L. and X.C. designed and made all figures. H.J. and X.C. designed and constructed the two-photon imaging device. R.D., X.L., S.L., J.G. and H.J. analyzed data. R.D., X.L., J.L., B.C., H.S. and X.C. wrote the manuscript with the help of all authors.

Additional Information

Competing Interests: The authors declare that they have no competing interests.

Publisher's note: Springer Nature remains neutral with regard to jurisdictional claims in published maps and institutional affiliations.



Open Access This article is licensed under a Creative Commons Attribution 4.0 International License, which permits use, sharing, adaptation, distribution and reproduction in any medium or format, as long as you give appropriate credit to the original author(s) and the source, provide a link to the Creative Commons license, and indicate if changes were made. The images or other third party material in this article are included in the article's Creative Commons license, unless indicated otherwise in a credit line to the material. If material is not included in the article's Creative Commons license and your intended use is not permitted by statutory regulation or exceeds the permitted use, you will need to obtain permission directly from the copyright holder. To view a copy of this license, visit <http://creativecommons.org/licenses/by/4.0/>.

© The Author(s) 2017